

Many-body Chern number from statistical correlations of randomized measurements

Ze-Pei Ciani,^{1,2} Hossein Dehghani,^{1,2} Andreas Elben,^{3,4} Benoît Vermersch,^{3,4,5}
Guanyu Zhu,⁶ Maissam Barkeshli,^{1,7} Peter Zoller,^{3,4} and Mohammad Hafezi^{1,2}

¹Joint Quantum Institute, College Park, 20742 MD, USA

²The Institute for Research in Electronics and Applied Physics,
University of Maryland, College Park, 20742 MD, USA

³Center for Quantum Physics, University of Innsbruck, Innsbruck A-6020, Austria.

⁴Institute for Quantum Optics and Quantum Information of the Austrian Academy of Sciences, Innsbruck A-6020, Austria.

⁵Univ. Grenoble Alpes, CNRS, LPMCM, 38000 Grenoble, France.

⁶IBM T.J. Watson Research Center, Yorktown Heights, New York 10598, USA.

⁷Condensed Matter Theory Center, Department of Physics,
University of Maryland, College Park, 20742 MD, USA

(Dated: July 21, 2022)

One of the main topological invariants that characterizes several topologically-ordered phases is the many-body Chern number (MBCN). Paradigmatic examples include several fractional quantum Hall phases, which are expected to be realized in different atomic and photonic quantum platforms in the near future. Experimental measurement and numerical computation of this invariant is conventionally based on the linear-response techniques which require having access to a family of states, as a function of an external parameter, which is not suitable for many quantum simulators. Here, we propose an ancilla-free experimental scheme for the measurement of this invariant, without requiring any knowledge of the Hamiltonian. Specifically, we use the statistical correlations of randomized measurements to infer the MBCN of a wavefunction. Remarkably, our results apply to disk-like geometries that are more amenable to current quantum simulator architectures.

Introduction.— Topologically ordered systems are a class of gapped quantum phases of matter [1, 2], which can have robust topological ground-state degeneracy, and host excited states with fractional statistics, known as anyons [3]. These systems, unlike symmetry protected topological (SPT) phases that have short range entanglement, acquire long-range entanglement which makes them a suitable platform for realizing quantum computation [4, 5]. Paradigmatic examples of chiral topologically ordered systems are the fractional quantum Hall (FQH) states that in certain cases are characterized by the many-body Chern number (MBCN), as their topological invariant.

In recent years, the interest in engineering topological states of matter in synthetic quantum systems has substantially grown. Examples of such quantum simulators include neutral atoms [6], superconducting qubits [7, 8], photons [9], and more recently Rydberg atoms [10, 11]. With these developments, the benefit of having direct access to the wave function in quantum simulators opens new avenues to investigate and measure the topological properties. In the conventional condensed matter physics the detection of topological properties relies on the application of external probes and linear response framework, and similar schemes have been also proposed for the simulated matter [12–14]. Moreover, ancilla-based approaches have been proposed that involve a many-body Ramsey interferometry to measure the topological charge [15], and entanglement spectrum [16]. But the fact that the ancilla should be coupled to the entire system limits the applicability of such schemes. Recently, this question has been theoretically investigated in the context of SPT systems

[17–22], but the problem for topologically-ordered system has been relatively unexplored.

Here, we propose a novel method for the measurement of MBCN. Using our recent findings [23], we show that given a wave function on a disk-like geometry, for a single set of parameters, one can construct the MBCN by applying certain operators on the wave function, without knowledge of the Hamiltonian. This should be contrasted

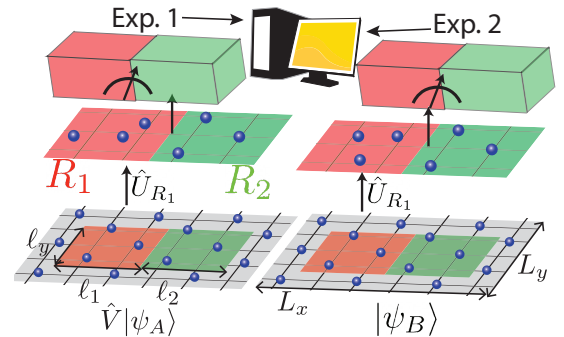


FIG. 1: The randomized measurement scheme. We define two regions R_1 (red) and R_2 (green) in the lattice with side length $\ell_1 \times \ell_y$ and $\ell_2 \times \ell_y$ respectively. We prepare two identical wave functions $|\psi_A\rangle$ and $|\psi_B\rangle$ in experiment A and B respectively. The local unitary operator \hat{V} is applied in the region R_1 in the exp. 1. Subsequently, the random unitary \hat{U}_{R_1} is applied in the region R_1 on both wave functions. The projective measurements on the particle occupation basis are performed on regions R_1 and R_2 in both experiments. The MBCN can be inferred from the statistical correlation between the randomized measurement results in experiment A and experiment B.

with the common situation where one requires a family of many-body wave functions, e.g., different twist angles on a torus. Importantly, such a construction allows one to perform the measurements using random unitaries [24–26]. Our scheme requires only a single wave function at a given time, for the same set of parameters, as schematically shown in Fig. 1. In other words, in each experimental realization, one requires only a single copy of the system, and simultaneous access to several identical copies of the wave function is not required. Therefore, this scheme can be easily implemented with the state of the art ultracold atoms, Rydberg arrays and circuit-QED platforms.

First, in the context of topological quantum field theory (TQFT) [27], we interpret and generalize the polarization formula for the MBCN [23]. We demonstrate that by introducing two symmetry defects, in the space-time manifold, one can evaluate the MBCN, as an expectation value of symmetry defect operators. This allows us to effectively change the boundary conditions of the wave function. Then, by cutting and gluing space-time manifolds, we show that topologically non-trivial space-time manifolds, such as a torus, can be obtained from a given wave function on a rectangular geometry. Such operations can be obtained by applying a SWAP operator between two subregions [21]. Similar to the Renyi entropy, where the expectation of the SWAP operator can be evaluated using a single copy of the wave function at a time, we show how such space-time surgery can be implemented in an experimental setting. Importantly, we show that the symmetry defects can be implemented by post-processing the data.

As a prerequisite for our protocol, we need to know the number of flux quanta that must be adiabatically inserted into a region of the system before a topologically trivial excitation is obtained [23]. As another feature of our protocol, we note that the amplitude of the SWAP expectation value decreases exponentially with the subregions area, in the absence of spatial symmetries. Moreover, the number of randomized measurements increases exponentially with the system size. Therefore, for both reasons, our protocol is particularly suitable for Noisy Intermediate-Scale Quantum (NISQ) devices [28].

Many-Body Chern Number.— In order to introduce the MBCN, we first consider a full multiplet of s topologically degenerate ground states on a torus. The wave functions are $\Psi_\alpha(\phi_x, \phi_y)$ defined on a torus geometry, with length L_x and L_y along the x and y directions, respectively. Here $\alpha = 1, \dots, s$ and we consider abelian quantum Hall states with Hall conductance $\sigma_{xy} = \frac{e^2}{h} \frac{p}{q}$, where p and q are co-prime integers and the parameter $s = q$. In this case, the parameter s is the number of flux quanta that has to be inserted before a topologically trivial excitation is obtained. We note that in general, the parameter s can be different from q when the degenerate ground state subspace is composed of multiple topological sectors. [45].

The twisted boundary conditions are defined as $\hat{t}_j(L_k \hat{k}) \Psi(\phi_x, \phi_y) = e^{i\phi_k} \Psi(\phi_x, \phi_y)$, where $k = x, y$ and $\hat{t}_j(\vec{r})$ being the magnetic translation operator of the j th particle along the direction \vec{r} . The MBCN of a FQH system is of the form [29]

$$C = \frac{1}{2\pi i} \int_0^{2\pi s} d\phi_x \int_0^{2\pi} d\phi_y \mathcal{F}(\phi_x, \phi_y), \quad (1)$$

where $\mathcal{F}(\phi_x, \phi_y) = \langle \partial_{\phi_x} \Psi_\alpha | \partial_{\phi_y} \Psi_\alpha \rangle - \langle \partial_{\phi_y} \Psi_\alpha | \partial_{\phi_x} \Psi_\alpha \rangle$ is the Berry curvature obtained from adiabatically varying the twist angle boundary conditions (ϕ_x, ϕ_y) , for a single wave function $|\Psi_\alpha\rangle$.

Alternatively, one can obtain the MBCN, when the wave function is given only as a function of one twist angle. Specifically, let $|\Psi_\alpha(\theta_x)\rangle$ be the ground state wave function in the presence of a flux through the x direction $\oint dx A_x = \theta_x$, and we take the flux in the y direction to be zero, $\oint dy A_y = 0$. We note that for the following argument, one can also consider a cylinder instead of a torus. Following Resta [30], we define the polarization operator as $R_y = \prod_{x,y} e^{i \frac{2\pi y}{L_y} \hat{n}(x,y)}$, where the product is taken over the whole system. We then compute

$$\mathcal{T}(\theta_x, s) = \langle \Psi(\theta_x) | R_y^s | \Psi(\theta_x) \rangle. \quad (2)$$

Adiabatically changing θ_x is equivalent to applying an electric field E_x , which induces a current in the y direction due to the Hall conductivity, which corresponds to a changing polarization along the \hat{y} direction. The MBCN therefore can be obtained as

$$C = \frac{1}{2\pi} \frac{d}{d\theta_x} \arg \mathcal{T}(\theta_x, s). \quad (3)$$

We note that equation above converges to the MBCN in the thermodynamic limit. For systems with finite size, a more robust result can be obtained by averaging over the twist angle: $C = \frac{1}{2\pi} \oint d\theta_x \frac{d}{d\theta_x} \arg \mathcal{T}(\theta_x, s)$. The Hall conductivity corresponds to $\sigma_H = \frac{C}{s} \frac{e^2}{h}$.

We note Eq. (1) and Eq. (2) are equivalent to each other and require toridal and cylindrical geometries, respectively. While there are theoretical proposals to implement such geometries [31, 32], an experimental realization remains challenging.

TQFT generalization of Resta Formula.— We interpret and generalize the polarization formula (2) using the TQFT formalism and the Chern-Simons response theory. The low-energy response of the system can be encoded in an effective action for the background electromagnetic gauge field A , such that the TQFT partition function on a space-time manifold M is given by,

$$\mathcal{Z}(M, A) = \mathcal{Z}(M, 0) e^{i \frac{p}{q} S_{CS}[A]}. \quad (4)$$

The Chern-Simons response action is given by $S_{CS}[A] = \frac{1}{4\pi} \int_M \epsilon^{\mu\nu\lambda} A_\mu \partial_\nu A_\lambda$, where $\mu = t, x, y$. The space-time

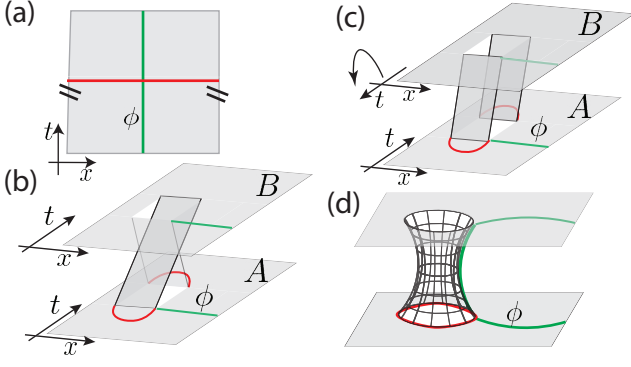


FIG. 2: (a) The space-time manifold of the $\mathcal{Z}(M, A)$ in Eq. (4), without showing the y axis. The green line represents the symmetry defects A_x and the red line corresponds to A_t . (b) The SWAP operator \hat{S}_{R_1} creates a branch cut in the region R_1 that connects the space time between system A and system B. The red and the green curves depict the operator \hat{V} and $\hat{W}(\phi)$ respectively. (c) A π rotation around the x axis in the system B maps the branch cut in (b) to a space time cylinder which is topologically equivalent to (d).

manifold M is $S^2 \times S^1$, where y and t are on the sphere S^2 and x is on the circle S^1 . Note that $x - y$ plane forms a torus. The twisted boundary condition required in the wave functions of Eq.(2) can be realized by applying $A_x = \theta_x \delta(x)$ and $A_y = 0$. We interpret Resta's polarization operator as an application of an electric field along the y direction at $t = 0$ and therefore $A_t = \frac{2\pi s y}{\ell_y} \delta(t)$. Under these conditions, the partition function is given by $\mathcal{Z}(M, A) = \mathcal{Z}(M, 0) e^{iC\theta_x}$, where $C = sp/q = p$. The background gauge fields in Eq. (4) form two symmetry defects which are wrapped around two distinct non-contractible loops on the manifold M , as shown in Fig. 2(a).

Now instead of measuring the MBCN on the $x - y$ torus, here we cut and glue the space-time manifold in TQFT to construct the partition function on a topologically non-trivial manifold, by starting with the state on simple space manifolds. This allows us to create two non-contractible loops on a disk geometry. We start from two identical wave functions $|\psi_A\rangle |\psi_B\rangle$. We apply the SWAP operation $\hat{S}_{R_1^A, R_1^B}$ between the two wave functions in the region R_1 as shown in Fig. 1. For an infinitesimal time interval ϵ , the SWAP operation glues the space-time manifold from $t = \mp \epsilon$ in A to $t = \pm \epsilon$ in B, respectively, as shown in Fig. 2(b). If we perform a π -rotation on the manifold of B along the \hat{x} axis, it becomes clear that the two required non-contractible loops are formed, as shown in the Fig. 2 (c) and (d). These non-contractible loops are used to apply the symmetry defects of the gauge potential A_t and A_x in this synthetic non-trivial topology.

Now, we make a connection between the TQFT and the microscopic theory to explicitly express the symmetry defects in Fig. 2 in terms of the system operators.

These symmetry defects are local in time and can be simply constructed by the local density operator $\hat{n}(x, y)$. Specifically, the operators that represent the polarization and the twist angle are

$$\hat{V}_R = \prod_{(x,y) \in R} e^{i \frac{2\pi s y}{\ell_y} \hat{n}(x,y)}, \quad \hat{W}_R(\theta_x) = \prod_{(x,y) \in R} e^{i \hat{n}(x,y) \theta_x}. \quad (5)$$

Now the MBCN can be obtained as the expectation value of the SWAP operator, which constructs the non-trivial space-time, and the above operators. Specifically,

$$\mathcal{T}(\theta_x) = \langle \psi_A | \langle \psi_B | \hat{V}_{R_1^A}^\dagger \hat{W}_{R_2^B}^\dagger(\theta_x) \hat{S}_{R_1^A, R_1^B} \hat{W}_{R_2^A}(\theta_x) \hat{V}_{R_1^A} | \psi_A \rangle | \psi_B \rangle, \quad (6)$$

where $R_i^{A(B)}$ is the i th region of the wave function $|\psi_{A(B)}\rangle$, $\hat{S}_{R_1^A, R_1^B}$ is the swap operation between the two copy of the wave function and $\mathcal{T}(\theta_x) \propto e^{iC\theta_x}$. Therefore, the winding number of $\arg[\mathcal{T}(\theta_x)]$ corresponds to the MBCN. We note that while our TQFT derivation of this formula is applicable to cylindrical geometries, extensive numerical simulations indicates that the same formula can also be applied to disk-like geometries [23].

Randomized Measurement Scheme.— We now present the experimental protocol to measure the MBCN via random measurements. Eq. (6) involves the SWAP operator between two copies of the wave function, and the expectation value can be obtained by performing a beam-splitter interaction between the two copies and a parity measurement [33–36]. In contrast, we show that a random measurement protocol requires only a single wave function, at a given time. Our key observation is that, without the symmetry defect operators, Eq.(6) is reminiscent of the second Renyi entropy expression and its evaluation through the SWAP operator expectation value, which can be extracted using randomized measurement [24]. Here, we need to generalize that scheme to incorporate the symmetry defect operators.

Let us consider a two-dimensional square lattice system with open boundary condition. Eq. (6) involves non-local SWAP operations between two replica of the wave functions. It can be performed through the following two randomized measurements as described in Fig. 1.

We start by preparing the wave function $|\psi\rangle$ in the open boundary condition. We first apply the operator \hat{V}_{R_1} on the state in the experiment A. We then perform the random unitary operation \hat{U} and the measurements on the occupation probability in the region R_1 and R_2 for both experiment A and B. The random unitary operations are sampled from an approximate unitary 2-design [37, 38]. After repeating the measurement N_M times, we obtain the probability distribution over the occupation basis $|b\rangle$. The results of the two experiments are $P_U^V(b) = |\langle b | \hat{U} \hat{V} | \psi \rangle|^2$ and $P_U(b') = |\langle b' | \hat{U} | \psi \rangle|^2$ respectively. We repeat the two experiments with different random unitary operations \hat{U} for N_U times. The statistical

correlation of the measurement results in the experiment A and B gives

$$\tilde{\mathcal{T}}(\theta_x) = \sum_{\{b\}} \sum_{\{b'\}} O_{b,b'}(\theta_x) \overline{P_U^V(b)P_U(b')}, \quad (7)$$

where the bar, $\overline{\cdots}$, means the average over the random unitaries from an approximate unitary 2-design. The coefficient $O_{b,b'}(\theta_x) = \delta_{N_1(b), N_1(b')} \mathcal{D}_b(-\mathcal{D}_b)^{\delta_{b,b'}-1} e^{i[N_2(b)-N_2(b')]\theta_x}$, where $N_1(b)$ and $N_2(b)$ are the number of particles of the basis state $|b\rangle$ in the region R_1 and R_2 respectively and $\mathcal{D}_b = \binom{\ell_1 \ell_y}{N_1(b)}$. Since $\tilde{\mathcal{T}}(\theta_x) = \mathcal{T}(\theta_x)$ for an ensemble average over a unitary 2-design [46], the winding number of the measurement result $\arg[\tilde{\mathcal{T}}(\theta_x)]$ gives the Chern number \tilde{C} .

In the following, we consider the randomized measurement scheme for system with non-trivial Chern number with finite number of N_U and number of projective measurements N_M for each realization of randomized measurement.

Numerical results. – We present the measurement of MBCN for bosonic fractional quantum Hall states with filling $\nu = 1/2$. We consider hard-core boson on the $N_x \times N_y$ square lattice in the open boundary condition, with a magnetic tunneling Hamiltonian of the form

$$H_t = -J \sum_{x,y} (\hat{a}_{x+1,y}^\dagger \hat{a}_{x,y} + e^{-i\Phi x} \hat{a}_{x,y+1}^\dagger \hat{a}_{x,y}) + \text{h.c.}, \quad (8)$$

where $\hat{a}_{x,y} (\hat{a}_{x,y}^\dagger)$ is the bosonic annihilation (creation) operator on site (x,y) , $\Phi = 2\pi/q$ is the magnetic flux on each plaquette. The ground state is known to be a FCI phase, with the MBCN $C = 1$ [39, 40].

In Fig. 3(a), we first show that the MBCN of this phase can be extracted, using the SWAP operator formula, Eq. (6). We observe that the correct quantized value $\tilde{C} = 1$ can be obtained, when the region size is larger than the magnetic length of the system, which is less than a lattice spacing in our case.

Then, in Fig. 3(b-d), we show that the MBCN can be extracted using randomized measurement (Eq.(7)). In order to implement random unitaries, we apply quench dynamics [25]. We consider the number conserving random quench unitary operation $\hat{U} = \prod_{k=1}^{\eta} e^{-iH_{q_k}T}$, where η is the depth of the random quench, T is the time step of each quench. The k th quench Hamiltonian is of the form

$$H_{q_k} = -J \sum_{\langle i,j \rangle, i,j \in R_1} (a_i^\dagger a_j + \text{h.c.}) + \sum_{i \in R_1} \Delta_i^k \hat{n}_i, \quad (9)$$

where Δ_i^k is a Gaussian distributed random number with mean zero and standard deviation Δ . It has been shown that when the magnitude of Δ is comparable to T^{-1} and J , the random quench unitary operator gives the approximate 2-design unitary [25].

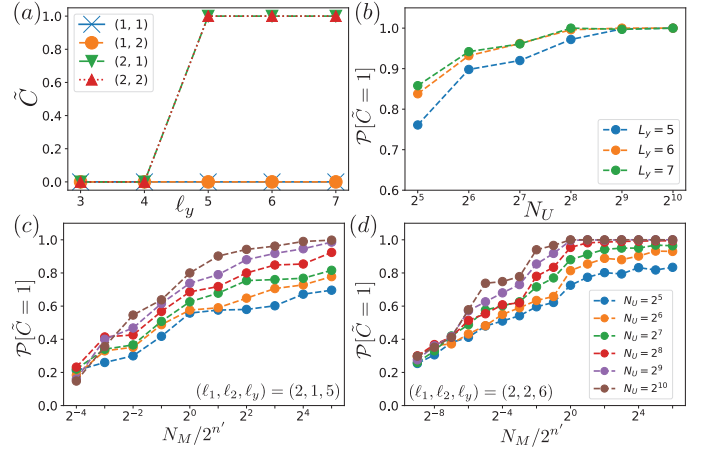


FIG. 3: Simulation results for Eq. (6) and (7), for the FCI phase with $C = 1$. (a) Obtained MBCN by Eq. (6) for various region size (ℓ_1, ℓ_2) and ℓ_y with $N_x = 6$, $N_y = 8$, labeled with different markers. (b) Probability of obtaining the expected MBCN ($\mathcal{P}[\tilde{C} = 1]$) from Eq. (7), using randomized measurements, as a function of the number of random unitary operations N_U with $N_M = \infty$. Region sizes are taken to be $\ell_1 = \ell_2 = 2$. (c, d) Probability of obtaining the expected MBCN versus number of measurements N_M , for two sets of region sizes. For all panels, $J = 1$, and $\Phi = 2\pi/3$. the probability $\mathcal{P}[\tilde{C}]$ is computed by averaging over 500 times independent randomized measurement results. Random quench parameters are $\eta = 20$, $\Delta = J$, $T = J^{-1}$ and $n' = 0.5n_1 + n_2$.

The performance of the randomized measurement is characterized by the probability of obtaining the correct MBCN $\mathcal{P}[\tilde{C} = 1]$. In Fig. 3(b), we consider the limit of $N_M \rightarrow \infty$, the performance of the randomized measurement weakly depends on the number of qubits in the measurement region R_1 and R_2 . In Fig. 3(c) and (d), the shot-noise of the measurements are taken into account. When the number of measurements N_M is of the same order of magnitude as $2^{n'}$, where $n' = 0.5n_1 + n_2$, and n_1 and n_2 are the number of sites in the region R_1 and R_2 respectively, the probability $\mathcal{P}[\tilde{C} = 1]$ starts to saturate. The factor $2^{0.5n_1}$ originates from the birthday paradox scaling of the randomized measurement in the region R_1 [24] and the factor 2^{n_2} is contributed by the shot-noise of the number operator measurement in the region R_2 . The randomized measurements can be realized in the current and near-term experimental platform. For example, in the circuit QED architecture with 10kHz repetition rate, each randomized measurement can be performed within a few minutes.

Adiabatic preparation of FCI. In order to experimentally realize the above FCI state, one can start by a Mott insulator state, by adding a trapping potential in form of a superlattice $V_{\text{trap}} = M \sum_{x,y} (-1)^{y+p_x} \hat{n}_{x,y}$, where and $p_x = \text{floor}(x/q)$ [39, 40]. Specifically, the Mott insulator for large trapping strength M , can be adiabatically melted into a FCI state by decreasing the strength

M . In Fig. 4, we consider an adiabatic process with $M(t) = M_0(1 - t/T_{ad})$, where M_0 is the initial trapping strength and T_{ad} is the adiabatic preparation time. The energy gap remains open in the process of adiabatic preparation, as shown in Fig. 4(b). For slow enough sweep, the overlap between the instantaneous ground state and the adiabatic wave function remains higher than 0.999 for $T_{ad} = 100J^{-1}$, as shown in Fig. 4(c). In Fig. 4(d), we show that the randomized measurement results agree with the theoretical values, in both trivial and topological limits. However, if the sweep time is not in the adiabatic limit, e.g., $T_{ad} = 1J^{-1}$ as in Fig. 4(c) and (d), then the system deviates from the FCI phase.

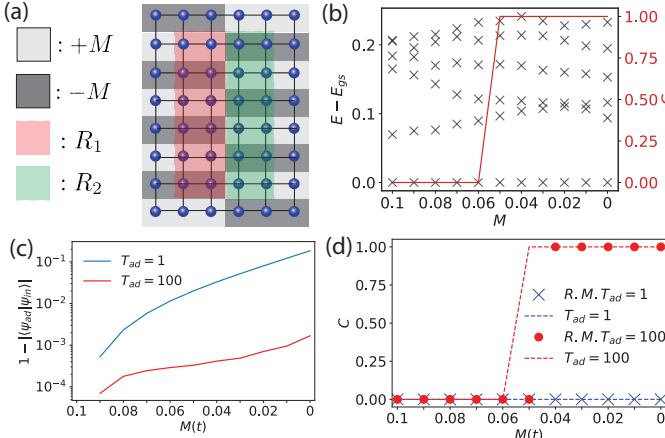


FIG. 4: Adiabatic preparation of FCI and measurement of MBCN by varying a trapping potential. (a) Schematics of the system considered in the simulation, with open boundary condition and $N_x = 6$, $N_y = 8$. Region lengths are $\ell_1 = 2$, $\ell_2 = 2$, $\ell_y = 6$ and $\Phi = 2\pi/3$. The potential energy is $-M/+M$ in the dark/bright regions, respectively. (b) The energy spectrum, and the corresponding MBCN as a function of M . (c) The fidelity $1 - |\langle\psi_{in}|\psi_{ad}\rangle|$, where $|\psi_{in}\rangle$ is the instantaneous eigenstate and the $|\psi_{ad}\rangle$ is the adiabatic wave function prepared by linearly decreasing the trapping strength M , with the preparation time T_{ad} . (d) The MBCN randomized measurement results with parameters $N_U = 1024$, $N_M = 2^{n'}$, $\eta = 20$, $\Delta = 1$ and $T = 1$.

Outlook.— Our work opens up a new avenue for creating non-trivial topology on space-time manifold, using the SWAP operation. It is particularly intriguing that the SWAP operation can be implemented by random unitaries in the NISQ devices. More broadly, quantum simulators are poised to realize topologically-ordered states that might not occur in a conventional electronic matter. Given this opportunity, it is important to develop measurement methods that go beyond linear response formalism. For example, it is interesting to investigate whether the application of SWAP operator through randomized measurement can be used to probe other topological characterizations, such as modular matrices [41], topological entanglement entropy [42, 43] and the order

parameter of the symmetry enriched topological phases [44].

Acknowledgments.— ZC thanks Hsin-Yuan Huang for helpful discussion about randomized measurement. BV thanks C. Repellin for discussions. ZC, HD, and MH were supported by AFOSR FA9550-16-1-0323, FA9550-18-10161, ARO W911NF-15-1-0397. HD, MH thank the hospitality of the Kavli Institute for Theoretical Physics, supported by NSF PHY-1748958. MB is supported by NSF CAREER (DMR-1753240), Alfred P. Sloan Research Fellowship. ZC, HD, MH, and MB acknowledge the support of NSF Physics Frontier Center at the Joint Quantum Institute. AE, BV and PZ were supported by the European Union’s Horizon 2020 research and innovation programme under Grant Agreement No. 817482 (PASQuanS) and No. 731473 (QuantERA via QTFLAG) and by the Simons Collaboration on Ultra-Quantum Matter, which is a grant from the Simons Foundation (651440, P. Z.).

- [1] Xiao-Gang Wen. Topological orders in rigid states. *International Journal of Modern Physics B*, 4(02):239–271, 1990.
- [2] Xiao-Gang Wen. Colloquium: Zoo of quantum-topological phases of matter. *Rev. Mod. Phys.*, 89: 041004, Dec 2017.
- [3] Frank Wilczek. Quantum mechanics of fractional-spin particles. *Phys. Rev. Lett.*, 49:957–959, Oct 1982.
- [4] A.Yu. Kitaev. Fault-tolerant quantum computation by anyons. *Annals of Physics*, 303(1):2 – 30, 2003. ISSN 0003-4916.
- [5] Chetan Nayak, Steven H. Simon, Ady Stern, Michael Freedman, and Sankar Das Sarma. Non-abelian anyons and topological quantum computation. *Rev. Mod. Phys.*, 80:1083–1159, Sep 2008.
- [6] N. R. Cooper, J. Dalibard, and I. B. Spielman. Topological bands for ultracold atoms. *Rev. Mod. Phys.*, 91: 015005, Mar 2019.
- [7] Andrew A Houck, Hakan E Türeci, and Jens Koch. On-chip quantum simulation with superconducting circuits. *Nature Physics*, 8(4):292, 2012.
- [8] Pedram Roushan, Charles Neill, Anthony Megrant, Yu Chen, Ryan Babbush, Rami Barends, Brooks Campbell, Zijun Chen, Ben Chiaro, Andrew Dunsworth, et al. Chiral ground-state currents of interacting photons in a synthetic magnetic field. *Nature Physics*, 13(2):146–151, 2017. doi: 10.1038/nphys3930.
- [9] Tomoki Ozawa, Hannah M Price, Alberto Amo, Nathan Goldman, Mohammad Hafezi, Ling Lu, Mikael C Rechtsman, David Schuster, Jonathan Simon, Oded Zilberberg, et al. Topological photonics. *Reviews of Modern Physics*, 91(1):015006, 2019.
- [10] Logan W Clark, Nathan Schine, Claire Baum, Ningyuan Jia, and Jonathan Simon. Observation of laughlin states made of light. *arXiv preprint arXiv:1907.05872*, 2019.
- [11] Antoine Browaeys and Thierry Lahaye. Many-body physics with individually controlled rydberg atoms. *Nature Physics*, pages 1–11, 2020.

- [12] Cecile Repellin and Nathan Goldman. Detecting fractional chern insulators through circular dichroism. *Physical review letters*, 122(16):166801, 2019.
- [13] Duc Thanh Tran, Alexandre Dauphin, Adolfo G Grushin, Peter Zoller, and Nathan Goldman. Probing topology by “heating”: Quantized circular dichroism in ultracold atoms. *Science advances*, 3(8):e1701207, 2017.
- [14] Luca Asteria, Duc Thanh Tran, Tomoki Ozawa, Matthias Tarnowski, Benno S Rem, Nick Fläschner, Klaus Sengstock, Nathan Goldman, and Christof Weitenberg. Measuring quantized circular dichroism in ultracold topological matter. *Nature physics*, 15(5):449–454, 2019.
- [15] Fabian Grusdt, Norman Y Yao, D Abanin, Michael Fleischhauer, and E Demler. Interferometric measurements of many-body topological invariants using mobile impurities. *Nature communications*, 7:11994, 2016.
- [16] Hannes Pichler, Guanyu Zhu, Alireza Seif, Peter Zoller, and Mohammad Hafezi. Measurement protocol for the entanglement spectrum of cold atoms. *Physical Review X*, 6(4):041033, 2016.
- [17] Marcel den Nijs and Koos Rommelse. Preroughening transitions in crystal surfaces and valence-bond phases in quantum spin chains. *Phys. Rev. B*, 40:4709–4734, Sep 1989.
- [18] Frank Pollmann and Ari M. Turner. Detection of symmetry-protected topological phases in one dimension. *Phys. Rev. B*, 86:125441, Sep 2012.
- [19] Jutho Haegeman, David Pérez-García, Ignacio Cirac, and Norbert Schuch. Order parameter for symmetry-protected phases in one dimension. *Phys. Rev. Lett.*, 109:050402, Jul 2012.
- [20] Ken Shiozaki and Shinsei Ryu. Matrix product states and equivariant topological field theories for bosonic symmetry-protected topological phases in (1+1) dimensions. *Journal of High Energy Physics*, 2017(4):100, Apr 2017. ISSN 1029-8479.
- [21] Ken Shiozaki, Hassan Shapourian, Kiyonori Gomi, and Shinsei Ryu. Many-body topological invariants for fermionic short-range entangled topological phases protected by antiunitary symmetries. *Phys. Rev. B*, 98:035151, Jul 2018.
- [22] Andreas Elben, Jinlong Yu, Guanyu Zhu, Mohammad Hafezi, Frank Pollmann, Peter Zoller, and Benoît Vermersch. Many-body topological invariants from randomized measurements in synthetic quantum matter. *Science advances*, 6(15):eaaz3666, 2020.
- [23] Hossein Dehghani, Ze-Pei Cui, Maissam Barkeshli, and Mohammad Hafezi. Manuscript in preparation.
- [24] A. Elben, B. Vermersch, C. F. Roos, and P. Zoller. Statistical correlations between locally randomized measurements: A toolbox for probing entanglement in many-body quantum states. *Phys. Rev. A*, 99:052323, May 2019. doi: 10.1103/PhysRevA.99.052323.
- [25] B. Vermersch, A. Elben, M. Dalmonte, J. I. Cirac, and P. Zoller. Unitary n -designs via random quenches in atomic hubbard and spin models: Application to the measurement of rényi entropies. *Phys. Rev. A*, 97:023604, Feb 2018.
- [26] Hsin-Yuan Huang, Richard Kueng, and John Preskill. Predicting many properties of a quantum system from very few measurements. *arXiv preprint arXiv:2002.08953*, 2020.
- [27] Edward Witten. Quantum field theory and the jones polynomial. *Communications in Mathematical Physics*, 121(3):351–399, Sep 1989. ISSN 1432-0916.
- [28] John Preskill. Quantum computing in the nisq era and beyond. *Quantum*, 2:79, 2018.
- [29] Qian Niu, D. J. Thouless, and Yong-Shi Wu. Quantized hall conductance as a topological invariant. *Phys. Rev. B*, 31:3372–3377, Mar 1985.
- [30] Raffaele Resta. Quantum-mechanical position operator in extended systems. *Phys. Rev. Lett.*, 80:1800–1803, Mar 1998.
- [31] Hwanmun Kim, Guanyu Zhu, James V Porto, and Mohammad Hafezi. Optical lattice with torus topology. *Physical review letters*, 121(13):133002, 2018.
- [32] Mateusz Lacki, Hannes Pichler, Antoine Sterdyniak, Andreas Lyras, Vassilis E Lembessis, Omar Al-Dossary, Jan Carl Budich, and Peter Zoller. Quantum hall physics with cold atoms in cylindrical optical lattices. *Physical Review A*, 93(1):013604, 2016.
- [33] A. J. Daley, H. Pichler, J. Schachenmayer, and P. Zoller. Measuring entanglement growth in quench dynamics of bosons in an optical lattice. *Phys. Rev. Lett.*, 109:020505, Jul 2012.
- [34] Dmitry A. Abanin and Eugene Demler. Measuring entanglement entropy of a generic many-body system with a quantum switch. *Phys. Rev. Lett.*, 109:020504, Jul 2012.
- [35] Rajibul Islam, Ruichao Ma, Philipp M Preiss, M Eric Tai, Alexander Lukin, Matthew Rispoli, and Markus Greiner. Measuring entanglement entropy in a quantum many-body system. *Nature*, 528(7580):77–83, 2015.
- [36] Adam M Kaufman, M Eric Tai, Alexander Lukin, Matthew Rispoli, Robert Schittko, Philipp M Preiss, and Markus Greiner. Quantum thermalization through entanglement in an isolated many-body system. *Science*, 353(6301):794–800, 2016.
- [37] Benoît Collins and Piotr Śniady. Integration with respect to the haar measure on unitary, orthogonal and symplectic group. *Communications in Mathematical Physics*, 264(3):773–795, 2006.
- [38] Zbigniew Puchała and Jarosław Adam Miszcza. Symbolic integration with respect to the haar measure on the unitary group. *arXiv preprint arXiv:1109.4244*, 2011.
- [39] Mohammad Hafezi, Anders Søndberg Sørensen, Eugene Demler, and Mikhail D Lukin. Fractional quantum hall effect in optical lattices. *Physical Review A*, 76(2):023613, 2007.
- [40] Johannes Motruk and Frank Pollmann. Phase transitions and adiabatic preparation of a fractional chern insulator in a boson cold-atom model. *Physical Review B*, 96(16):165107, 2017.
- [41] Guanyu Zhu, Mohammad Hafezi, and Maissam Barkeshli. Quantum Origami: Transversal Gates for Quantum Computation and Measurement of Topological Order. *arXiv:1711.05752*, November 2017.
- [42] Alexei Kitaev and John Preskill. Topological entanglement entropy. *Physical review letters*, 96(11):110404, 2006.
- [43] Michael Levin and Xiao-Gang Wen. Detecting topological order in a ground state wave function. *Physical review letters*, 96(11):110405, 2006.
- [44] José Garre-Rubio and Sofyan Iblisdir. Local order parameters for symmetry fractionalization. *New Journal of Physics*, 21(11):113016, 2019.
- [45] We define a topological sector to consist of all the degenerate ground states which can be related to each other

under the operation of quantized flux insertion in the x and y cycles of a torus [23].

[46] See supplementary for the derivation.

Supplementary : Derivation of Eq. (7) In this supplementary, we derive Eq.(7) in the main text, which allows us to extract the MBCN from the statistical correlations of randomized measurements.

We start by considering two arbitrary density matrices ρ_A and ρ_B with dimension \mathcal{D} . As shown in [24], the expectation value of the SWAP operator can be implemented by the 2-design random unitary operations of the form

$$\text{tr}(\rho_A \otimes \rho_B \hat{\mathbb{S}}_{A,B}) = \mathcal{D} \sum_{s_1, s_2} (-\mathcal{D})^{1-\delta_{s_1, s_2}} \overline{P_U^A(s_1) P_U^B(s_2)}, \quad (10)$$

where $P_U^\alpha(s) = \text{tr}(U \rho_\alpha U^\dagger |s\rangle\langle s|)$ and $\alpha = A, B$.

Notice that the right hand side of the above equation can be written as

$$\begin{aligned} & \mathcal{D} \sum_{s_1, s_2} (-\mathcal{D})^{1-\delta_{s_1, s_2}} \overline{P_U^A(s_1) P_U^B(s_2)} \\ &= \mathcal{D} \sum_{s_1, s_2} (-\mathcal{D})^{1-\delta_{s_1, s_2}} \\ & \times \overline{\text{tr}(|s_1\rangle\langle s_1| \otimes |s_2\rangle\langle s_2| U \otimes U \rho_A \otimes \rho_B U^\dagger \otimes U^\dagger)} \\ &= \text{tr}(U^\dagger \otimes U^\dagger \hat{O} U \otimes U \rho_A \otimes \rho_B), \end{aligned} \quad (11)$$

where $\hat{O} = \mathcal{D} \sum_{s_1, s_2} (-\mathcal{D})^{1-\delta_{s_1, s_2}} |s_1\rangle\langle s_1| \otimes |s_2\rangle\langle s_2|$.

By using the 2-design property of the random unitary operation, we obtain

$$\begin{aligned} \overline{U \otimes U \hat{O} U^\dagger \otimes U^\dagger} &= \frac{1}{\mathcal{D}^2 - 1} (\text{tr}(\hat{O}) - \frac{1}{\mathcal{D}} \text{tr}(\mathbb{S}_{A,B} \hat{O})) \hat{I} \\ &+ \frac{1}{\mathcal{D}^2 - 1} (\text{tr}(\hat{\mathbb{S}}_{A,B} \hat{O}) - \frac{1}{\mathcal{D}} \text{tr}(\hat{O})) \hat{\mathbb{S}}_{A,B}, \end{aligned} \quad (12)$$

Since $\text{tr}(\hat{O}) = \mathcal{D}$ and $\text{tr}(\hat{O} \hat{\mathbb{S}}_{A,B}) = \mathcal{D}^2$, we arrive at equation (10).

Using equation (10), now we can rewrite $\mathcal{T}(\theta_x)$ defined in the main text, in terms of statistical correlations,

$$\mathcal{T}(\theta_x) = \langle \tilde{\psi}_A | \langle \psi_B | \hat{W}_{R_2^B}^\dagger(\theta_x) \hat{\mathbb{S}}_{R_1^A, R_1^B} \hat{W}_{R_2^A}(\theta_x) | \tilde{\psi}_A \rangle | \psi_B \rangle, \quad (13)$$

where $|\tilde{\psi}_A\rangle = \hat{V}_{R_1^A} |\psi\rangle$.

Since the operators $\hat{W}_{R_2^A}$ and $\hat{W}_{R_2^B}$ are diagonal in the particle occupation basis, we can apply it after projective measurements. Specifically, we use the following identity

$$\begin{aligned} \mathcal{T}(\theta_x) &= \sum_{s_{R_2}} e^{iN(s_{R_2})\theta_x} e^{-iN(s'_{R_2})\theta_x} \\ &\times \langle \tilde{\psi}_A | \langle \psi_B | \hat{\mathbb{S}}_{R_1^A, R_1^B} \hat{P}_{s_{R_2}}^A \hat{P}_{s'_{R_2}}^B | \tilde{\psi}_A \rangle | \psi_B \rangle, \end{aligned} \quad (14)$$

where s_{R_2} is the basis of particle number configuration in the region R_2 , $N(s)$ is the number of particle in the basis state $|s\rangle$ and $\hat{P}_{s_{R_2}}^{A(B)}$ is the projector that projects

the particle configuration in the region R_2 into the state s_{R_2} .

Now, we perform the partial trace operator on wave functions A and B and only keep the region R_1 . Correspondingly, we can rewrite (14) as,

$$\begin{aligned} \mathcal{T}(\theta_x) &= \sum_{s_{R_2}} e^{iN(s_{R_2})\theta_x} e^{-iN(s'_{R_2})\theta_x} \\ &\times \text{tr}(\rho_{A;s_{R_2}} \otimes \rho_{B;s_{R_2}} \hat{S}_{R_1^A, R_1^B}), \end{aligned} \quad (15)$$

where the reduced density matrix is defined as $\rho_{p;s_{R_2}} = \text{tr}_{R/R_1}(\hat{P}_{s_{R_2}}|\psi_p\rangle\langle\psi_p|)$, where $p = A, B$.

For the ground state of a number conserving Hamiltonian, the reduced density matrix $\rho_{p;s_{R_2}}$ can be written as the direct sum of the density matrix with different number of particles. Therefore, $\rho_{p;s_{R_2}} = \bigoplus_{k=0}^{\infty} \rho_{p;s_{R_2}}^k$, where $\rho_{p;s_{R_2}}^k$ is the reduced density matrix with k particle in the region R_1 .

The SWAP operation $\hat{S}_{R_1^A, R_1^B}$ is a number conserving

operation and it can also be factorized into the direct sum of SWAP operations with different number of particles sectors $\hat{S}_{R_1} = \bigoplus_{k=0}^{\infty} \hat{S}_{R_1}^k$. Equation (15) can be simplified as

$$\begin{aligned} \mathcal{T}(\theta_x) &= \sum_{s_{R_2}} e^{iN(s_{R_2})\theta_x} e^{-iN(s'_{R_2})\theta_x} \\ &\times \bigoplus_{k=0}^{\infty} \text{tr}(\rho_{A;s_{R_2}}^k \otimes \rho_{B;s_{R_2}}^k \hat{S}_{R_1}^k). \end{aligned} \quad (16)$$

The SWAP operator in the k -particle sector can be implemented by equation (10) with the random unitary acting on the k -particle sector \hat{U}_k which can be implemented with the random quench dynamics with number conserving Hamiltonian. By replacing the SWAP operation in equation (16) by the random unitary operation defined in equation (10), we reach equation (6) in the main text.